Chapter 5

Non-enzymatic electrochemical sensing of hydrogen peroxide (H_2O_2) and glucose using NiO-MoS_2 electrode

---

In Chapter 4, a non-enzymatic amperometric glucose sensing approach has been discussed by using CuO/PEDOT-MoS_2 based hybrid nanostructure. The sensor demonstrated a reliable detection of glucose with very low LOD and good sensitivity. The fabrication of the nanocomposite film was performed through an electrochemical deposition technique which allows uniform and defect free growth of the nanoparticles. Though it is a robust and controlled way of material synthesis, it provides very less control over the morphology of the synthesized nanosystem. Besides, several properties of the material are largely influenced by the morphology. In this work, we have intended to fabricate a sensor probe having 2D morphology of the host electrocatalyst. Furthermore, use of the same electrocatalyst for detection of multiple analytes can extend potential applicability of the sensor offering versatility and broad utility.

5.1. Introduction

As discussed in Chapter 1 (Section 1.4), monitoring of glucose and H_2O_2 levels in the body is of paramount importance as it yields crucial information regarding body metabolism. Previous chapter has explained a rapid and sensitive determination of glucose by electrochemically fabricated CuO/PEDOT-MoS_2 based sensor probe. Here, CuO is the host catalyst and PEDOT-MoS_2 acts as a supporting material providing synergic increment in the electrocatalytic activity and sensing ability. However, the performance of a sensor probe can be enhanced significantly by altering the morphology of the host electrocatalyst. Besides, 2D metal-oxide nanostructures have attained immense interest owing to their exceptional properties, such as high aspect ratio (surface-to-volume), tailored reactivity due to nanoscale confinement effect and presence of large number of active sites for charge adsorption [201, 202]. Unlike copper, nickel also has high abundancy, superior stability along with easy synthesis procedure. It also exhibits remarkable redox activities towards H_2O_2 and glucose [203, 204]. Thus, a 2D nanostructure of NiO nanosheet (NS) could be a

suitable choice as a host material for detection of both the analytes. In earlier three chapters, electrochemical deposition technique was followed for preparing the composite electrode systems. The primary limitation of electrochemical deposition technique lies in its limited ability to control the morphology of the deposited material [205]. Whereas a required morphology can be optimized by following hydrothermal route and optimized chemical synthesis procedure. As highlighted in the results obtained in Chapter 4, the incorporation of layered MoS_2 can certainly augment the redox activity of the metal-oxide nanosheet towards H_2O_2 and glucose. In this work, we have followed a hydrothermal method for synthesizing a composite of 2D NiO and MoS_2 nanosheets for non-enzymatic determination of both H_2O_2 and glucose. Here, our objective is to develop a novel electrocatalyst with tailored morphology that can execute broad utility by detecting multiple analytes with high sensitivity and good selectivity.

5.2 Experimental

5.2.1. Synthesis of MoS_2 nanosheet

Similar hydrothermal route was followed for the synthesis of MoS_2 nanosheets as described in section 3.2.2, in Chapter 3. But this time the concentration of the precursors has been reduced in the solution to avoid uneven nucleation and growth of crystals. For this, 1.24 g ammonium molybdate tetrahydrate with 2.28 g of thiourea were dissolved 36 ml of DI water under vigorous stirring for 30 min to form a homogeneous solution. The solution was transferred into a 50 ml autoclave and heated at a temperature of 220^0C for 24 h. The autoclave was allowed to cool naturally down to room temperature. Afterwards, the black precipitate was washed several times with distilled water and ethanol and finally dried overnight at a temperature of 60^0C.

5.2.2. Synthesis of NiO-MoS_2 nanosheet composite

NiO-MoS_2 nano composite was synthesized by employing a hydrothermal route. At first, 0.1 M $NiCl_2.6H_2O$ solution was prepared in 20 mL solvent comprised of ethanol and DI water in 1:1 ratio. 0.15 g of the as prepared MoS_2 was added in the above solution and stirred for 1 h until a homogeneous dispersion is obtained. Then, 0.2 g polyvinylpyrrolidone (PVP) along with 10 mL ethylene glycol (EG) were added in the mixture under constant stirring of @500 rpm. The pH of the above mixture was adjusted at 11 by adding 25% ammonia (NH_3) solution. Afterwards, the final solution was transferred into a 50 mL teflon-lined autoclave and heated in a hot-air oven at a temperature of 140^oC for 12 h. After the hydrothermal treatment, the autoclave was allowed to cool down naturally. Finally, the

obtained sample was centrifuged at 7000 rpm to collect the precipitate followed by washing several times with ethanol and pure water. The powder was obtained after drying overnight at a temperature of 60^{o}C followed by calcination at a temperature of 600^{o}C for 1 h [206].

5.2.3. Fabrication of sensor electrode

Firstly, 3 mg of the as-prepared NiO-MoS_2 NPs were mixed with 10 wt% of a binder, poly-vinylidene fluoride (PVDF). The binder and the electroactive specimen (NiO-MoS_2) were then dispersed in 50 µL N-Methyl-2-Pyrrolidone (NMP). They were properly mixed in the form of slurry and pasted over the 0.5 cm^2 area of the Indium Tin Oxide (ITO) electrode. They were dried at a temperature of 60^{0}C in hot air oven and then stored in a desiccator until next use.

5.3 Results and discussion

5.3.1. Structural and morphological studies

The XRD patterns of the synthesized nanoparticles are shown in Figure 5.1(a). In the 1st diffractogram, the characteristic peaks appearing at 2θ ~ 14.5^o, 32.5^o and 57.3^o resemble the (002), (100) and (110) diffraction planes of MoS_2, respectively. In case of NiO-MoS_2 system, the intense peaks arising at 2θ ~ 37.1^o, 43.1^o, 62.8^o and 75.4^o correspond to the (111), (200), (220) and (311) diffraction planes of NiO (JCPDS no. 47-1049), respectively [207]. The small diffraction peak observed at 2θ ~ 26.6^o indicates the presence of NiO_x phase in the system under study [208]. However, the (002) peak of MoS_2 in the NiO-MoS_2 system maintains its characteristic position, whereas the presence of the composite leads to a discernible suppression of the other MoS_2 peaks [209]. Figure 5.1(b) shows the FT-IR spectrum of the synthesized NPs. Here, the vibrational bands observed at ~ 600 cm^{-1} corresponds to the Mo-S bond vibration (black spectrum) [210]. In the NiO-MoS_2 composite, the broad absorption band appeared in the region 500-600 cm^{-1} corresponds to Ni-O stretching vibration, and the MoS_2 vibrational band notably got suppressed due to the formation of complex composite structure. In the EDX response of Figure 5.1(c), the appearance of the inner shell absorption peaks of Ni, Mo, O and S confirms the presence of the all the constituent elements in the prepared nanocomposite system. This can also be realized from the elemental mapping of the specimen performed under scanning electron microscope (SEM) as shown in the inset image of Figure 5.1 (c). The arrangement of the NiO NSs with curled edges can be traced in the field emission scanning electron microscopy (FESEM) image of Figure 5.1(d). These well separated smooth NiO NSs are seemed to be distributed uniformly over the nanocomposite surface facilitating high

catalytic surface area. In Figure 5.1(e), one can view the distribution of surface rough MoS_2 sheets which seemed to be stacked in and over the NiO NSs. For clear visualization, few of the MoS_2 NSs are marked under dotted white boundary lines, whereas the NiO NSs are shown under the dotted yellow circular boundary. Morphologically, these layered TMDC nanostructures are distinct from the smooth NiO NSs by their surface roughness. The TEM micrograph of the corrugated NiO-MoS_2 nanosheets system is shown in Figure 5.1(f). The transparent part of the TEM image elucidates the distribution of the thin NiO NSs having folded silk-like morphology. However, the long spike-like dark parts of this micrograph designates the curled edges of the folded NSs [211, 212]. The appearance of the distinct, circular rings in the SAED pattern of Figure 5.1(g) would indicate polycrystalline nature of the synthesized nanosystem.

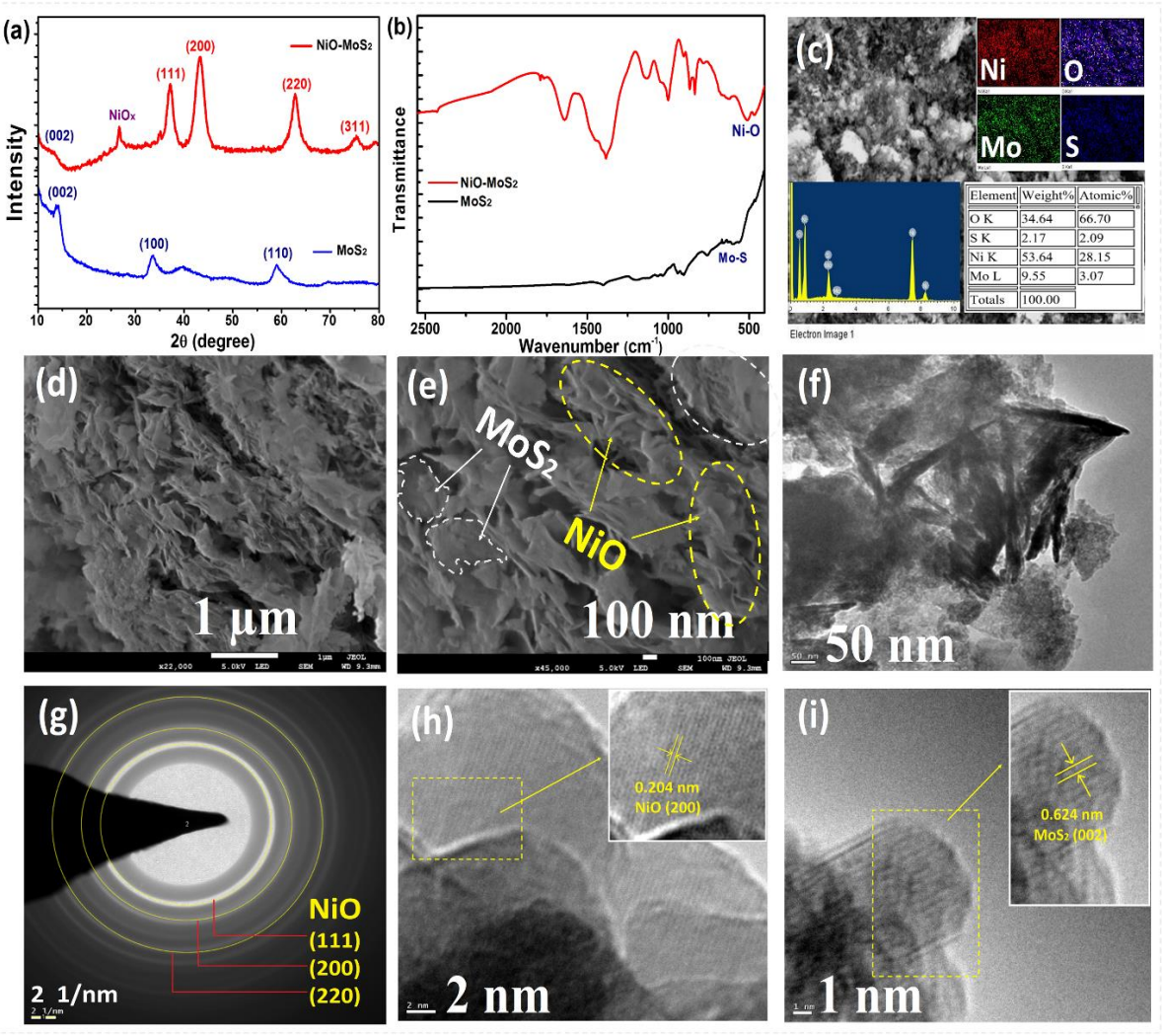

Figure 5.1: (a) XRD, (b) FT-IR, (c) EDX, elemental mapping responses, (d, e) FESEM images, (f) TEM micrograph, (g) SAED pattern and (h, i) HRTEM images of the NiO-MoS_2 nanocomposite system

The interplanner spacing (*d*-spacing) values corresponding to different diffraction planes have been estimated to be 0.252 nm, 0.204 nm and 0.158 nm that correspond to the (111), (200) and (220) planes of NiO, respectively. These obtained *d*-spacings values of NiO are quite indifferent from the theoretical values [213]. Due to the low atomic percentage of MoS_2 in our system, the diffraction rings corresponding to MoS_2 sheets have not appeared in the SAED pattern. To further assess the MoS_2 in the micrograph, high-resolution TEM (HRTEM) images of the NiO-MoS_2 based system have been performed as depicted in Figure (h) and (i), where one can clearly trace the lattice fringes. By using ImageJ software, fast Fourier transformation (FFT) have been performed in the selected area of the HRTEM micrographs for estimating the *d*-spacing values. The inset image of Figure 5.1(h) resembles (200) plane of NiO with a fringe width of 0.204 nm. While, a *d*-spacing value of 0.624 nm have been estimated from Figure 5.1(i) designating (002) plane of MoS_2 [68]. Thus, the HETEM images suggest the presence of both NiO and MoS_2 in the synthesized nanocomposite system.

5.3.2. Cyclic voltammetry (CV) study

Cyclic voltammetry experiment was performed in a three-electrode system by taking NiO-MoS_2/ITO as working electrode, a platinum wire as a counter electrode and Ag/AgCl as reference electrode. In Figure 5.2(a), the CV responses were taken at a scan rate of 20 mV/s under the potential window of -1.2V to 0.2 V w.r.t. the reference in 0.1 M PBS solution. In bare PBS solution, it doesn't show any reduction peak during the cathodic scan. But, upon addition of 0.1 mM H_2O_2 in the PBS solution, a prominent reduction peak can be observed around -1.1 V potential, which is represented by the red-coloured CV response in Figure 5.2(b). Appearance of this redox peak indicates that H_2O_2 is getting reduced by the NiO NPs, throughout this applied potential. The electrochemical reactions taken place during the redox process are as represented below [214]:

$$Ni^{2+}+H_2O_2 \rightarrow Ni^{3+}+{}^{*}OH+OH^{-} \quad (5.1)$$

$$Ni^{3+}+H_2O_2 \rightarrow Ni^{2+}+{}^{*}OOH+H^{+} \quad (5.2)$$

$$2H_2O_2 \rightarrow {}^{*}OH+{}^{*}OOH+H_2O \quad (5.3)$$

$${}^{*}OOH \rightarrow O_2+H^{+} \quad (5.4)$$

$$2H_2O_2 \rightarrow 2H_2O+O_2 \quad (5.5)$$

Here, Ni^{2+} state of NiO is oxidized to Ni^{3+} state during the cathodic scan of the CV cycle, and both these two oxidation states of Ni can separately perform half-cell reactions

with the dissolved H_2O_2, as denoted in equation (5.1) and (5.2). The full cell rection results in the formation of hydroxyl ($^*OH$) and hydroperoxyl ($^*OOH$) radicals along with water as by-product (Equation (5.3)). This $^*OOH$ radical is usually unstable and breaks into O_2 and H^+ ion. Finally, the resultant of (5.3) and (5.4) redox mechanisms yield H_2O and oxygen. The interfacial electron transfer process taking place during $Ni^{2+} \rightarrow Ni^{3+}$ results in the change in reduction current in the CV cycle, followed by appearance of prominent redox hump at -1.1 V potential. Afterwards, the height of the reduction peak current increases in that region when concentration of H_2O_2 is further increased in the solution, as can be seen in Figure 5.2(b). Here, upon each addition of H_2O_2, the height of the reduction peak current increases accordingly. This specifies the effective reduction mechanism of H_2O_2 occurring in the sensor electrode at -1.1 V potential, and from the change in reduction peak height, one can detect and quantify the amount of H_2O_2 present in the solution.

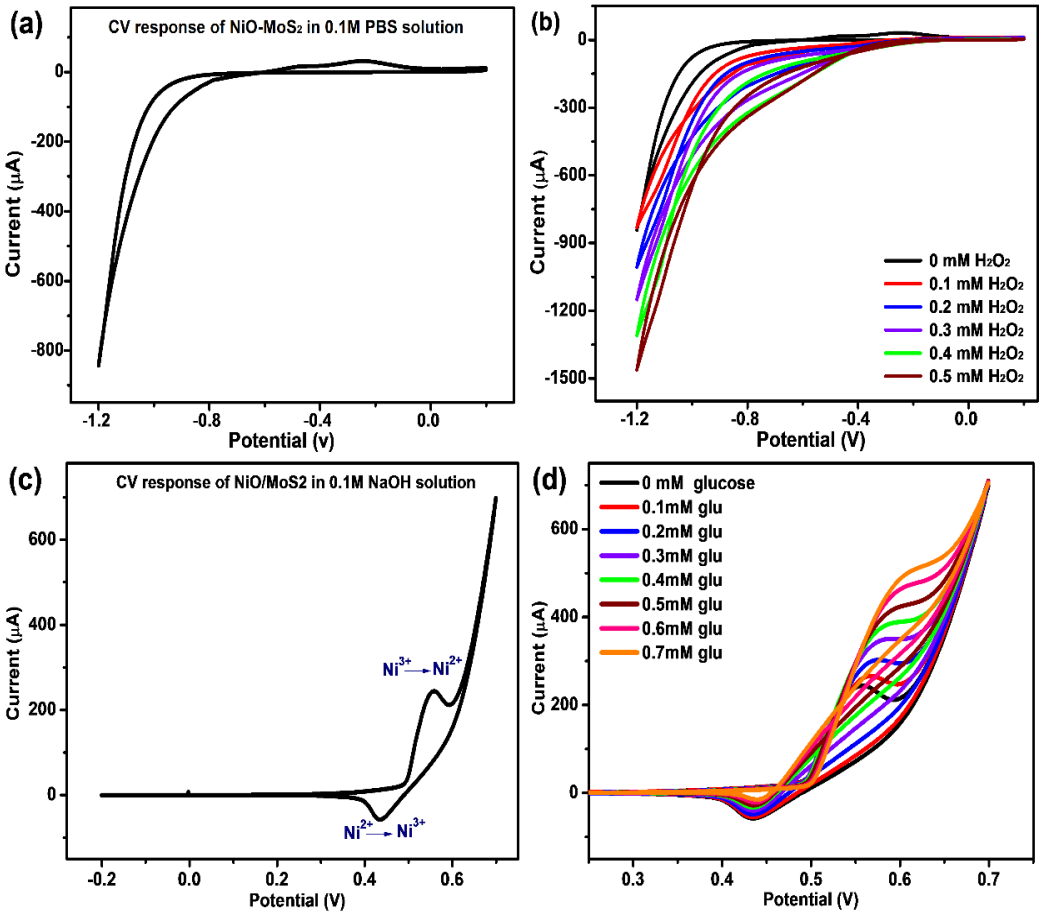

Figure 5.2: Cyclic voltammetry response of NiO-MoS_2 sensor electrode in (a) 0.1M PBS solution, (b) 0.1M PBS solution with varying H_2O_2 concentration, (c) 0.1M NaOH solution, (d) 0.1M NaOH solution with varying glucose concentration.

Figure 5.2(c) shows the CV response taken at a scan rate of 20 mV/s under the potential window of -0.2 V to +0.7 V in 0.1 M NaOH solution. The selection of the potential window primarily depends upon the redox activity of the sensor towards the analyte molecules. In our sensor, we considered the amperometric response generated during glucose oxidation for quantitative detection of glucose. So, the potential window is considered in the anodic region (positive potential region) such that the working electrode act as electron acceptor to oxidize glucose. Using NiO-MoS_2 based sensor, a good electrochemical activity has been attained in 0.1 M of NaOH. In absence of glucose, the respective oxidation and reduction peaks have appeared at a potential of ~0.55 V and ~0.45 V (Figure 5.2(c)), which correspond to the reversible conversions occurring between Ni^{2+} to Ni^{3+} states. When different amounts of glucose were added in the NaOH solution by varying the concentration from 0.1 mM to 0.7 mM, then a significant enhancement in the anodic current can be observed under the potential range of ~ (0.55 V- 0.6 V) indicating effective oxidation of glucose taking place in the electrode, as can be viewed in Figure 5.2(d). In this figure, the oxidation current increases regularly as well as the reduction current tends to abate slowly w.r.t. the added concentration of glucose in the solution that indicates excellent electrocatalytic activity of the NiO-MoS_2 based system for glucose oxidation [215]. Here, the reduction peaks appearing at ~0.45 V are attributed to the $Ni^{2+} \rightarrow Ni^{3+}$ conversions only. Whereas glucose oxidation occurring within the potential region of 0.55 V- 0.6 V has overlapped with the $Ni^{3+} \rightarrow Ni^{2+}$ conversion redox peak at 0.55 V. To be mentioned, when we say glucose is oxidized over the NiO based working electrode then it means that the active metal counterpart Ni has undergone reduction. As the electron generated from glucose oxidation is accepted by the Ni^{3+} state to complete the electrochemical process. Here, the glucose oxidation is carried out by the Ni^{3+} state of Ni, where the Ni^{2+} state of NiO is oxidized to nickel oxy hydroxide (Ni (OOH)) in the basic medium of NaOH solution, as depicted in equation (5.6). This Ni^{3+} state of Ni (OOH) can oxidise glucose to Glucolactone, followed by reduction of $Ni^{3+} \rightarrow Ni^{2+}$. Afterwards, upon hydrolysis, Glucolactone is transformed into gluconic acid, resulting the glucose oxidation reaction as: Glucose$\rightarrow$ Gluconic acid+H_2O. The electron transfer occurring throughout the redox process of equation (5.7) is responsible for the rise in oxidation current upon addition of glucose in the solution [216]. It has been found in both the cases that the prominent H_2O_2 reduction and stable glucose oxidation current would occur at -1.1 V and +0.6 V potential, respectively. These two potentials were employed as fixed bias potentials in the chronoamperometric experiments for the detection of H_2O_2 and glucose.

$$Ni^{2+} + OH^- \rightarrow Ni(OOH) + e^- \quad (5.6)$$

$$Ni^{3+} + Glucose + e^- \rightarrow Glucolactone + Ni^{2+} \quad (5.7)$$

$$Glucolactone \rightarrow Gluconic\ acid\ (hydrolysis) \quad (5.8)$$

5.3.3 Impedance spectroscopy study

The experimental set up for acquiring the EIS spectra of NiO-MoS_2 based sensor has identical configuration as mentioned in section 5.3.2. The EIS was performed by varying the frequency from 1 MHz to 1 Hz at a 0 V dc bias potential. The corresponding real and imaginary parts of the resultant impedance are plotted in the Nyquist plot as shown in Figure 5.3. Figure 5.3(a) depicts the EIS response of the sensor electrode in 0.1M PBS solution. In the Nyquist plot, the scattered points resemble the EIS response of the experimentally obtained data points. Whereas, the solid spectral line represents the fitted data which is obtained after fitting the experimental data points by using the equivalent Randle circuit shown in the inset figure. The meaning and significance of each parameter of the equivalent circuit have already been discussed in section 2.3.6. The values of the fitted parameters have been depicted in Table 5.1 in case of the NiO-MoS_2 system before and after the detection of glucose and H_2O_2. In Table 5.1, the increase in the R_{ct} value from 22.90 Ω to 32.58 Ω after addition of H_2O_2 in the PBS solution may be due to the formation of the by-product after reduction of H_2O_2 at the electrode interface which may have hindered the interfacial charge transfer. Again, in Figure 5.3(b), the EIS response of the fabricated sensor electrode was monitored in 0.1 M NaOH solution. Here, also the scattered points and solid lines corresponds to the experimental data points and fitted spectra, respectively. The inset figures represent the equivalent circuit and the magnified portion of the Nyquist plot at high frequency region. As can be seen from the values of fitted spectra that the R_{ct} value increases form 15.36 Ω to 23.25 Ω after addition of 0.1 mM glucose in the NaOH solution (Table 5.1). This is also because of the formation of gluconic acid as a by-product at the interface, which can partially block the redox process. However, the small R_{ct} value of NiO-MoS_2 substrate in both PBS and 0.1 M NaOH solution indicates an improved charge transfer kinetics of our as fabricated sensor. A decrease in the value of Q_2 can be observed in both cases after the addition of analyte in the solution, as can be seen in Table 5.1. This is because, addition of H_2O_2 and glucose leads to the faradic electron transfer at the interface during redox process, causing a diminution in the C_{dl} value. In the equivalent circuit, Q_3 is another CPE of low magnitude which may have emerged due to the space charge layers in between layered MoS_2 and NiO NS. The magnitude of Q_3

decreases after addition of the analytes, indication blocking nature of the generated byproducts, which eventually lead to the diminution in space charge density in between the nanosystems. Moreover, the Warburg impedance (W_3) arises due to the diffusion process taking place in the system. A significant increment in the W_3 parameter upon addition of H_2O_2 and glucose would suggest the diffusion of these analytes towards our system electrode in use.

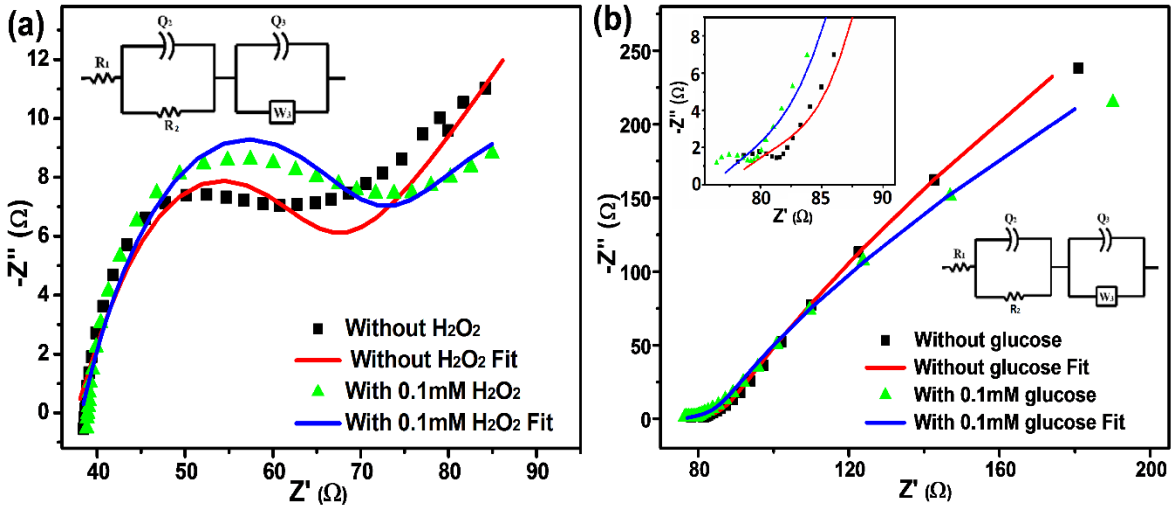

Figure 5.3: EIS response of NiO-MoS_2 sensor electrode in (a) 0.1 M PBS solution and (b) 0.1M NaOH solution, with an inset Nyquist plot showing the magnified view of the high frequency region.

Table 5.1: Fitted parameter of the Nyquist plot for the sensor electrode

NiO-MoS_2 electrode	**R_1** (Ω)	**R_2** (Ω)	**Q_2** ($\times 10^{-3}$F) η	**Q_3** ($\times 10^{-3}$F) η	**W_3** ($\times 10^{-3}$) $S.s^{1/2}$
In 0.1M PBS	37.40	22.90	27.24 η = 0.269	0.254 η = 0.658	0.107
0.1 mM H_2O_2 in PBS	38.22	32.58	22.16 η = 0.016	0.307 η = 0.601	16.09
In 0.1M NaOH	77.23	15.36	0.488 η = 0.936	5.14 η = 0.361	0.623
0.1 mM glucose in NaOH	76.07	23.25	0.380 η = 1	8.05 η = 0.355	0.962

5.3.4. Sensing of H_2O_2 and glucose by chronoamperometry

Figure 5.4(a) shows the chronoamperometric response captured for the sensor electrode in 0.1 M PBS solution at an applied dc bias potential of -1.1 V w.r.t. the reference, which is basically the H_2O_2 reduction potential estimated from the CV experiment. First, the chronoamperometry experiment was initiated until a stable baseline is observed in the *i-t* response. Then, H_2O_2 was added in the solution at varying concentration over different intervals of time, which lead to a proportional drop in current in the amperometric response due to the reduction of H_2O_2. Similarly, Figure 5.4(b) depicts the chronoamperometric response of NiO-MoS_2 based sensor in 0.1 M NaOH solution at an applied dc bias potential of +0.6 V which is the estimated potential for glucose oxidation. Here also, a noticeable increase in the amperometric current was observed after each subsequent addition of glucose in the solution.

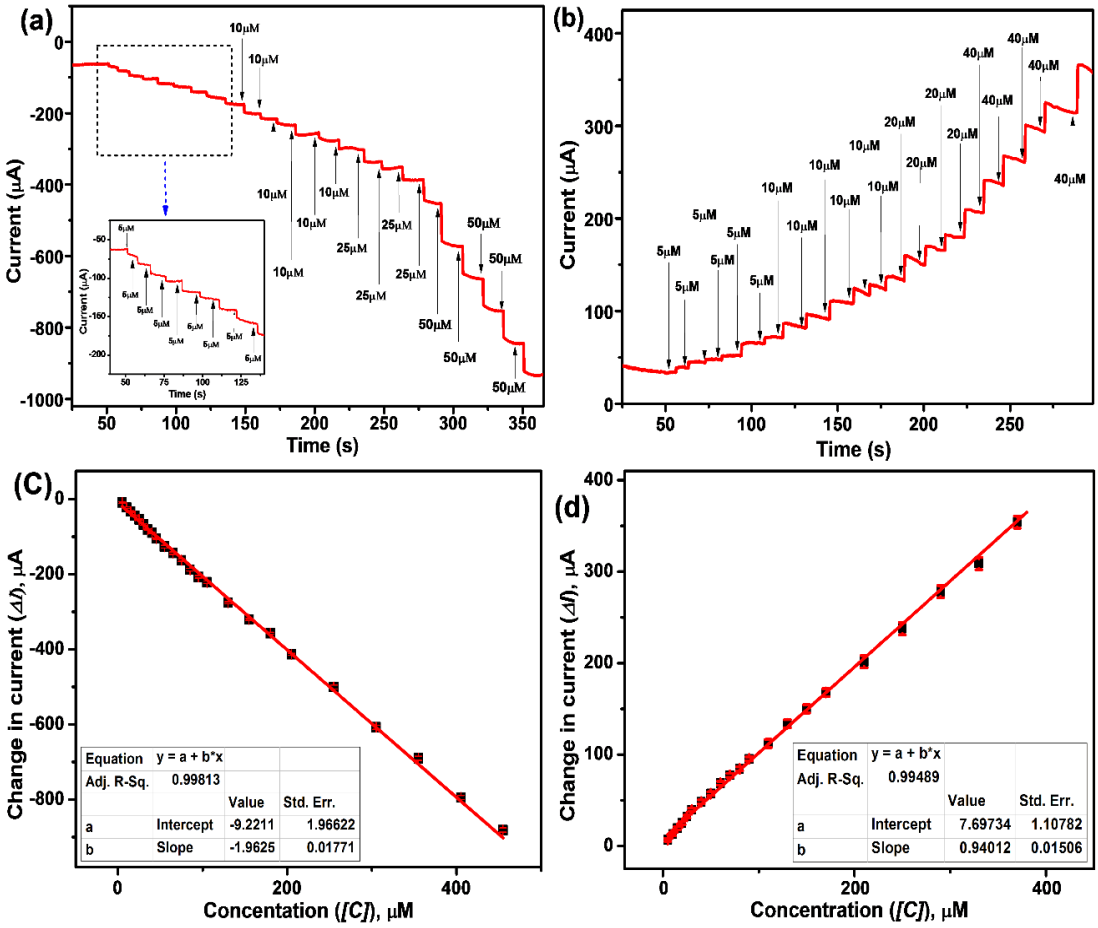

Figure 5.4: Chronoamperometric response of NiO-MoS_2 sensor electrode in (a) 0.1M PBS solution, (b) 0.1M NaOH solution. (c) ΔI vs. $\Delta[C]$ plot for H_2O_2 sensing, (d) ΔI vs. $\Delta[C]$ plot for glucose sensing.

The change in amperometric current (ΔI) corresponding to the added concentration ($\Delta[C]$) of H_2O_2 and glucose is plotted as depicted in Figure 5.4(c) and 5.4(d), respectively. The obtained data points of Figure 5.4(c) and 5.4(d) are fitted linearly for further calculation of the sensing parameters of the fabricated sensor. The calibration equation for the sensor towards sensing H_2O_2 and glucose are estimated to be, y = -1.962x-9.221 and y = 0.940x+7.697, respectively. The *LOD* corresponding to the linearly fitted data of Figure 5.4(c) has been obtained to be 3.00 μM and with a sensitivity value of 3925 $\mu A.mM^{-1}.cm^{-2}$ under the linear range of 5-455 μM in 0.1M PBS solution for detection of H_2O_2. Similarly, for sensing of glucose, the detection limit is calculated to be 3.53 μM having a sensitivity value of 1880 $\mu A.mM^{-1}.cm^{-2}$ over a wide linear range of 5-370 μM in 0.1 M NaOH solution.

5.3.5. Selectivity and reliability test

The selectivity aspect of our sensor electrode towards H_2O_2 and glucose was monitored by taking the chronoamperometric response in presence of other interfering molecules in the solution. Figure 5.5(a) represents the chronoamperometric response of the sensor in 0.1 M PBS solution at an applied dc bias potential of -1.1 V. Here, the current response did not show any observable change upon addition of ascorbic acid (AA), uric acid (UA) and glucose in the PBS solution; but a remarkable current shift was obtained upon addition of H_2O_2 in the solution. Similarly, the selectivity towards glucose was examined by another *i-t* response depicted in Figure 5.5(b), which was monitored at an applied dc bias potential of +0.6V in 0.1M NaOH solution. No significant current change has been observed on addition of ascorbic acid, uric acid and H_2O_2 in the solution. Nevertheless, an immense rise in oxidation current monitored after addition of glucose in the NaOH solution indicating the selective nature of the sensor. Thus, we can conclude that our prepared sensor electrode exhibits good selectivity towards H_2O_2 and glucose at certain applied dc bias potential.

(a) Detection of H_2O_2 in artificial urine sample

The reliability feature of the NiO-MoS_2 based sensor electrode for H_2O_2 detection was established by detecting the H_2O_2 concentration in the artificially prepared urine sample. The urine sample was prepared in the lab by following the standard protocol, upon mixing 0.36 gm urea, 0.15 gm sodium chloride (NaCl), 0.09 gm sodium phosphate (Na_3PO_4) and 0.04 gm creatinine in 20 mL DI water (pH is adjusted to 5.1) [217]. Then, the prepared urine sample was spiked with H_2O_2 at different concentrations. Detection of H_2O_2 level in the spiked urine sample was carried out by taking the chronoamperometric response of the senor probe in the PBS solution by applying a dc bias potential of -1.1 V. This was followed

by addition of different concentration of spiked urine sample in the solution, as shown in Figure 5.5(c). The substantial drop in reduction current observed in the amperometric response indicates that our prepared sensor electrode is capable of determining H_2O_2 level in the urine test sample. Afterwards, the as proposed regression equation, *viz.* $x = \frac{y+9.221}{|-1.962|}$ was used to determine the concentration of H_2O_2 level in the urine samples from the change in current value obtained in the amperometric curve of Figure 5.5(c). In this relation, y is the variation in current observed after the addition of spiked urine sample and x is the unknown concentration of the analyte. Table 5.2 shows the systematic comparison of the obtained concentration of H_2O_2 with the actual H_2O_2 level in the spiked sample. A low standard deviation of 0.69 µM indicates that the estimated values and the actual values of the concentration do not differ much from each other.

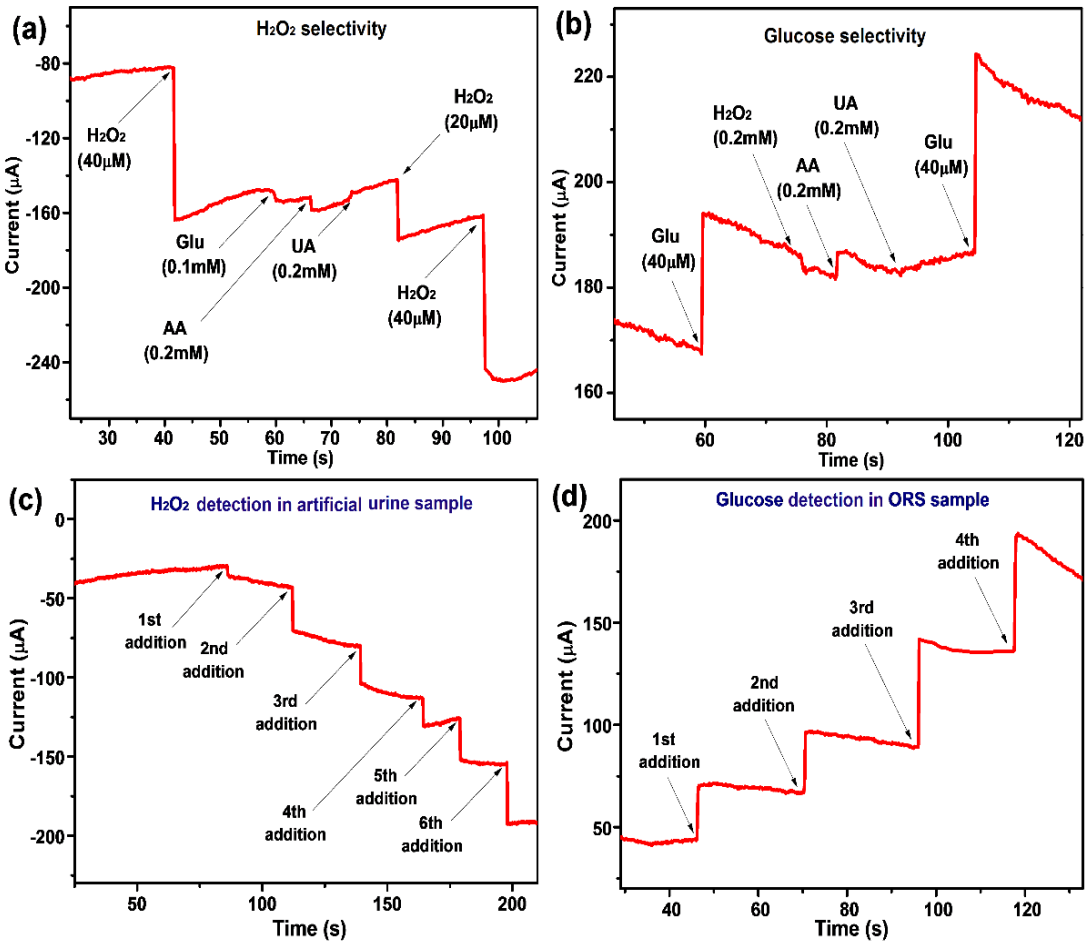

Figure 5.5: Selectivity feature of NiO-MoS_2 based sensor for (a) H_2O_2 sensing and (b) glucose sensing. Detection of (c) H_2O_2 in artificial urine sample and (d) glucose in ORS sample

(b) Detection of glucose in ORS sample

Similarly, the validity of the prepared sensor for detection of glucose in real samples was evaluated by testing the concentration of glucose in a commercially available ORS sample as described in section 4.3.8. Initially, aqueous solutions of ORS were prepared each having a different concentration of glucose. Then, the glucose levels in the prepared ORS samples were validated by employing our sensor module. This was accomplished by taking the chronoamperometric response of the NiO-MoS_2 based sensing unit in 0.1 M NaOH solution, and subsequently adding the prepared ORS samples into the solution. The unknown concentration of glucose in the prepared ORS samples were estimated by using the already established regression relation: $x = \frac{y-7.697}{0.940}$; where, y is the current variation occurring in the amperometric response of Figure 5.5(d) and x is the unknown concentration of glucose in the prepared ORS samples. The obtained values of glucose concentration in the ORS samples were compared with the corresponding real values, as depicted in Table 5.2 above. A low standard deviation of 0.54 µM suggests that the estimated values closely align with the actual values of the concentration, indicating a high level of accuracy and precision of the fabricated sensing unit.

Table 5.2: Detection of H_2O_2 and glucose in artificial urine and ORS samples

No. of addition	H_2O_2 detection in artificial urine sample				Glucose detection in ORS sample			
	$\|\Delta I\|$ (µA)	Estimated conc. ([C*]) (µM)	Actual conc. ([C]) (µM)	Error [ΔC] = ([C]-[C*]) (µM)	$\|\Delta I\|$ (µA)	Estimated conc. ([C*]) (µM)	Actual conc. ([C]) (µM)	Error [ΔC] = ([C]-[C*]) (µM)
1st	8.92	9.24	10	-0.76	30.53	24.29	25	-0.71
2nd	29.86	19.91	20	-0.09	32.06	25.63	25	+0.63
3rd	30.36	20.17	20	+0.83	54.81	50.12	50	+0.12
4th	20.77	15.28	15	+0.28	55.48	50.54	50	+0.54
5th	28.43	19.19	20	-0.81	--	--	--	--
6th	40.61	26.06	25	+0.94	--	--	--	--

5.3.6. Repeatability test

The repeatability feature of the NiO-MoS_2 based sensor towards the detection of H_2O_2 and glucose have been examined by performing the sensing experiments multiple times, as depicted in Figure 5.6 (a) and (b). The experimental procedure followed for this study is similar as mentioned in section 5.3.4. Detection of H_2O_2 was conducted independently for three times using chronoamperometric technique at an applied dc potential of -1.1 V in 0.1 M PBS solution. All the *i-t* responses obtained after H_2O_2 sensing are merged together as shown in Figure 5.6 (a). The similar nature of these responses validates the reproducible feature of our sensor for detection of H_2O_2. Again, we have independently performed the glucose sensing experiment upto four times by chrono-amperometric method in 0.1 M NaOH solution at an applied bias potential of +0.6 V. All the obtained *i-t* responses are merged together as shown in Figure 5.6 (b). The consistent trend observed in all the responses affirms the repeatability aspect of NiO-MoS_2 derived sensor for detection of glucose also.

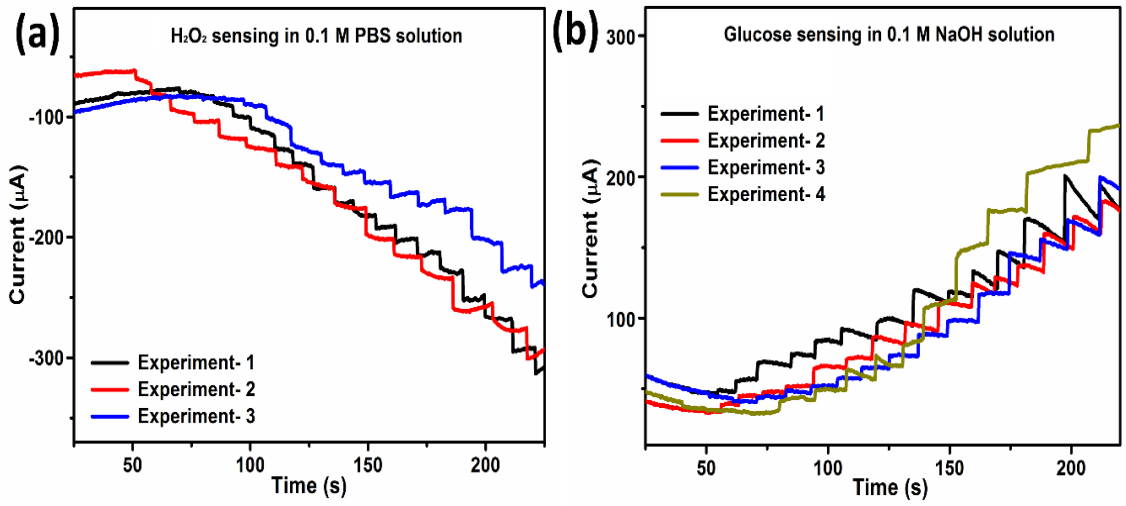

Figure 5.6: Repeatability test of NiO-MoS_2 based sensor for the detection of (a) H_2O_2, and (b) glucose

5.4 Conclusions

This work has illustrated the fabrication of a non-enzymatic sensor by using NiO and MoS_2 NS based composite. Structural, morphological studies and elemental mapping suggest the formation of NiO and MoS_2 based nanosheet system. Electrochemical studies illustrate that the fabricated sensor can effectively reduce H_2O_2 in 0.1 M PBS solution and oxidise glucose in 0.1 M NaOH solution at -1.1 V and +0.6 V applied dc bias potentials, respectively. Thus, detection of both H_2O_2 and glucose have been executed by using the as

designed sensor. The detection limit and sensitivity for detection of H_2O_2 was calculated to be 3 µM and 3925 µA $mM^{-1}cm^{-2}$, respectively under the linear range of 5-455 µM in 0.1 M PBS solution. While, a moderate *LOD* value of 3.53 µM and high sensitivity of 1880 µA. $mM^{-1}.cm^{-2}$ have been found for detection of glucose 0.1 M NaOH solution under the linear range of 5-370 µM. In addition, the sensor can deliver selective detection of the target analytes in both real and spiked samples. This metal oxide-TMDC based nanocomposite system offers a promising avenue for the development of highly sensitive non-enzymatic electrochemical sensors. The detection of multiple analytes using the same sensor is an interesting feature added to this work. The proposed sensor offered higher sensitivity values for detection of both H_2O_2 and glucose indicating high signal amplification. However, the observation of moderate *LOD* values stands out as primary limitation associated to this study. The traditional methods for material modifications have some limitations as one can hardly probe into the of lattice structures by following these methods. Whereas by using an ion beam technique, one can achieve a controlled and optimized modification. So, the impact of energetic ion beams on materials is an exciting field for exploration.